Available online at www.sciencedirect.com

ScienceDirect

Current Opinion in Electrochemistry

Review Article

# *Operando* methods: A new era of electrochemistry

Yao Yang[1,2,3,4], Julian Feijóo[1,3], Valentín Briega-Martos[5], Qihao Li[4], Mihail Krumov[4], Stefan Merkens[6], Giuseppe De Salvo[6], Andrey Chuvilin[6,7], Jianbo Jin[1], Haowei Huang[1], Christopher J. Pollock[8], Miquel B. Salmeron[9,10], Cheng Wang[11], David A. Muller[12,13], Héctor D. Abruña[4,13] and Peidong Yang[1,3,8,9,14]

**Abstract**

One of the grand challenges facing electrochemistry is to directly resolve the complex nature of (electro)catalyst active sites and capture real-time "*movies*" of reaction dynamics, *i.e.* "*watching chemistry in action*". The need for such fundamental understanding has stimulated the development of *operando*/*in situ* methods, which have greatly enhanced our ability to identify activity descriptors of electrocatalysts and establish structure–property relationships of energy materials. This review summarizes the frontiers of *operando* electrochemical liquid-cell scanning transmission electron microscopy and correlative synchrotron X-ray methods, which are complementary tools to comprehensively investigate reaction dynamics across multiple spatiotemporal scales. In an effort to encourage greater adoption of advanced *operando* methods by the general electrochemistry community, this review points out the need to benchmark electrochemistry in confined and heterogenous liquid environment with minimal beam-induced damage. We anticipate that multimodal *operando* methods will become indispensable for understanding interfacial reaction mechanisms for the broad chemistry and energy materials communities.

**Addresses**

[1] Department of Chemistry, University of California, Berkeley, CA, 94720, USA
[2] Miller Institute for Basic Research in Science, University of California, Berkeley, CA, 94720, USA
[3] Chemical Sciences Division, Lawrence Berkeley National Laboratory, Berkeley, CA, 94720, USA
[4] Department of Chemistry and Chemical Biology, Cornell University, Ithaca, NY, 14853, USA
[5] Forschungszentrum Jülich GmbH, Helmholtz-Institute Erlangen-Nürnberg for Renewable Energy (IEK-11), Cauerstr. 1, 91058, Erlangen, Germany
[6] Electron Microscopy Laboratory, CIC NanoGUNE BRTA, Tolosa Hiribidea 76, Donostia, San Sebastián, 20018, Spain
[7] Ikerbasque, Basque Foundation for Science, Bilbao, 48013, Spain
[8] Cornell High Energy Synchrotron Source, Cornell University, Ithaca, NY, 14853, USA
[9] Materials Sciences Division, Lawrence Berkeley National Laboratory, Berkeley, CA, 94720, USA
[10] Department of Materials Science and Engineering, University of California, Berkeley, CA, 94720, USA
[11] Advanced Light Source, Lawrence Berkeley National Laboratory, Berkeley, CA, 94720, USA
[12] School of Applied and Engineering Physics, Cornell University, Ithaca, NY, 14853, USA
[13] Kavli Institute at Cornell for Nanoscale Science, Cornell University, Ithaca, NY, 14853, USA
[14] Kavli Energy NanoScience Institute, Berkeley, CA, 94720, USA

Corresponding author: Yang, Yao (yaoyang1@berkeley.edu)

**Current Opinion in Electrochemistry** 2023, **42:**101403

This review comes from a themed issue on **Innovative Methods in Electrochemistry (2023)**

Edited by **Emmanuel Maisonhaute** and **Jay D.Wadhawan**

For a complete overview see the Issue and the Editorial

Available online 28 September 2023

https://doi.org/10.1016/j.coelec.2023.101403



**Keywords**

*Operando* methods, Electrochemical interfaces, Electrocatalysis, Energy materials, Scanning transmission electron microscopy, Synchrotron X-rays.

Electrochemistry lies at the interfaces among chemistry, physics and materials science and represents one of the more promising approaches for enhancing energy efficiency, mitigating environmental impacts and carbon emissions, and enabling renewable energy technologies, such as fuel cells, $CO_2$ and $N_2$ reduction, water splitting and post lithium-ion secondary batteries [1,2]. The past decades have witnessed the tremendous development in analytical instruments in the context of measurement science [3]. Recent advances in scanning transmission electron microscopy (STEM) and synchrotron X-ray methods have revived the field of electroanalytical chemistry [4]. Here, we review the latest breakthroughs of *operando*/*in situ* methods with an emphasis on electrons and X-rays as complementary structural probes of solid–liquid interfaces. For other analytical techniques,

interested readers are encouraged to read reviews on *operando/in situ* optical microscopy and spectroscopy (UV–Vis, IR and Raman), differential electrochemical mass spectrometry (DEMS), scanning electrochemical microscopy (SECM), scanning electrochemical cell microscopy (SECCM), nanoimpact electrochemistry and electrochemical quartz microbalance (EQCM) [1,4–8].

First, we would like to give a clear definition of *ex situ*, *in situ* and *operando*. *Ex situ* methods provide a baseline understanding of pristine or postmortem samples. *In situ* methods simulate one or some of the reaction conditions but still deviate from realistic (device-level) operating conditions. *Operando* methods emphasize achieving multiple experimental conditions to fully sustain a working (electro)catalyst in an operating device [5,8]. Given the term *in situ* has been widely used in the past decades and *operando* is just emerging and requires considerable efforts to achieve device-level operation, this review provides flexibility regarding the precise boundary between *in situ* and *operando* methods and serves primarily as a roadmap to inspire readers to contribute to the advancement of *operando* methods. For electrochemistry, *operando* methods are defined here as analytical techniques that provide a comparable driving force (applied potential) to achieve a comparable reaction rate (current density), relative to standard electrochemical cells [4]. This review will first introduce recent breakthroughs in developing multimodal *operando/in situ* methods [9,11], particularly *operando* electrochemical liquid-cell STEM (EC-STEM) and correlative synchrotron X-ray methods. Selected examples of representative STEM or TEM (S/TEM), hard and soft X-ray methods will be discussed in detail. Particular attention is paid to beam-induced effects on samples in liquid cells [12]. It remains necessary to convince the electrochemistry community that *operando* EC-STEM and X-ray methods can deliver comparable electrochemical results to bench-top electrochemical measurements.

Electrons and X-rays are complementary tools for probing electrochemical reaction dynamics at solid–liquid interfaces across multiple spatiotemporal scales. The customized electrochemical liquid cell serves as a multimodal platform to combine those two powerful structural probes (Schematic 1). In general, electron probes provide nm-to-atomic scale information of individual nanoparticles (NPs) in a localized environment, while synchrotron based X-rays interrogate a large ensemble of NPs with statistical analysis. For both electrons and X-rays, beam-induced damage needs to be minimized in order to reliably probe electrochemical reactions without perturbing them. Conventional TEM uses a parallel electron beam while STEM focuses an electron beam into a sub-Ångström probe, which scans across the sample and is then analyzed by an electron detector [13,14]. *Operando* EC-STEM enables

**Schematic 1**

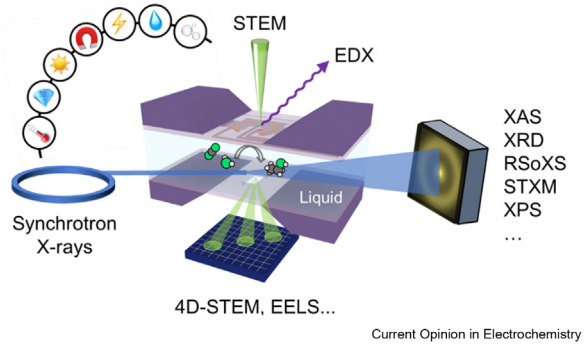


Multimodal *operando* STEM and correlative X-ray methods: A powerful complementary toolbox. The upper left schematic includes a variety of stimuli (temperature, pressure, light, magnetic fields, electrical bias, liquid or gas environment) that may alter (electro)chemical reaction dynamics at solid–liquid interfaces (Copyright by the authors).

quantitative electrochemistry and simultaneous acquisition of quantitative STEM imaging, four-dimensional (4D) diffraction imaging, electron energy loss spectroscopy (EELS) and energy dispersive X-ray (EDX) spectroscopy [9,15–17]. In comparision, synchrotron based X-rays are divided into hard X-rays (>5 keV), tender X-rays (1–5 keV) and soft X-rays (<1 keV). High-energy hard X-rays can penetrate mm or thicker samples in standard electrochemical cells or operating energy devices. Soft X-rays are more advantageous as a probe for surface and thin film electronic structures due to their large absorption cross-section and chemical sensitivity. *Operando* X-ray methods include X-ray absorption spectroscopy (XAS), X-ray diffraction (XRD), resonant soft X-ray scattering (RSoXS), scanning transmission X-ray microscopy (STXM), X-ray photoelectron spectroscopy (XPS), among others.

State-of-the-art *operando/in situ* S/TEM and X-ray studies are summarized in Table 1. Given the concise scope of this review, the table only includes reports that have demonstrated *operando/in situ* S/TEM or X-ray methods in liquid under electrochemical conditions. A comprehensive summary of early *operando/in situ* STEM and X-ray studies can be found in our early review [4]. Rows 2–5 cover the real- and reciprocal-space resolutions, temporal and energy resolutions of electron or X-ray probes in the presence of liquid. Rows 6–7 include the output information of chemical compositions and crystal structures. The ideal multimodal *operando* methods are expected to resolve morphological and compositional changes in real space and structural changes in reciprocal space at high spatiotemporal resolutions without beam damage in liquid. The overview of Table 1 delivers the important message that no single technique can possibly satisfy such an ideal requirement. Therefore, multimodal techniques are highly

**Table 1**

**Summary of state-of-the-art *operando*/*in situ* S/TEM and correlative X-ray methods in liquid under electrochemical conditions. Electrons and X-rays serve as complementary probes to study solid–liquid interfaces across multiple spatiotemporal scales.**

| *Operando* Methods in Liquid under Electro- chemical Conditions | Real-Space Resolution | Reciprocal-Space Resolution | Temporal Resolution | Energy Resolution | Chemical Composition | Crystal Structure |
|---|---|---|---|---|---|---|
| STEM imaging [9,15–24] | nm to atomic scalescale | No | Second-level | N/A | Quantitative imaging | No |
| 4D-STEM diffraction imaging [9,16,17] | nm to atomic scale | sub-Å | Seconds to minutes | N/A | No | Yes |
| STEM-EELS [22,24,28,59] | nm to atomic scale | No | Minute-level | ~0.5 eV (without monochromator) ~0.1 eV (with monochromator) | Yes | No |
| STEM-EDX [16,59] | nm-scale | No | Minutes to hours | ~100 eV | Yes | No |
| TEM imaging [21,31–36,59,71] | nm-scale | No | Milliseconds to seconds | N/A | No | No |
| Selected Area Electron Diffraction [35,59] | No | sub-Å | Milliseconds to seconds | N/A | No | Yes |
| Hard XAS (XANES) in conventional [36–42], HERFD [9,43,44] modes) | No | No | Seconds to minutes | ~1.5 eV (Conventional) 0.5–0.75 eV (HERFD) | Yes | No |
| Hard XAS (EXAFS) [9,36–44] | No | No | Minutes to hours | N/A | Yes | No |
| Hard XRD (CTR or XSWs) [46,47] | No | sub-Å | Milliseconds to seconds | N/A | No | Yes |
| Hard X-ray Microscopy (Coupled XRD or XRF) [48,50] | 2 μm | sub-Å | Minutes to hours | N/A | Yes | Yes |
| Soft XAS (TFY or TEY) [51–55] | No | No | Minutes to hours | ~0.1 eV | Yes | No |
| RSoXS Coupled Soft XAS [56] | No | sub-nm | Milliseconds to seconds | ~0.1 eV | Yes | Yes |
| Soft STXM [10,57] Coupled Soft XAS | 50 nm | No | Minutes to hours | ~0.1 eV | Yes | No |
| AP-XPS [58] | No | No | Minutes to hours | 0.1–0.5 eV | Yes | No |

desirable to provide comprehensive information and approach a complete understanding of complex solid–liquid interfaces [11]. Although aberration-corrected STEM imaging can routinely achieve sub-Å spatial resolution in vacuum, the imaging resolution of EC-STEM is often limited to a few nanometers by counting statistics, at a beam dose of 1–10 $e^{-}/Å^{2}$ or lower to reliably study beam-sensitive samples in liquid [12,15–17]. Similarly, despite recently developed electron detectors achieving a kHz-level or higher imaging frame rate (*i.e.* ms-level or higher temporal resolution), most S/TEM studies in liquid are limited to second-level temporal resolution in order to achieve a sufficiently high signal-to-noise ratio (SNR) when imaging nanoscale features in liquid. In other words, the spatial and temporal resolutions are often determined by the maximum beam dose allowed in liquid samples rather than instrumental resolutions. Recently, the maximum useable imaging speed (MUIS) has been proposed as a new information metric to integrate the spatial and temporal resolutions of electron detectors [14]. The MUIS, as a function of the SNR, determines the precision and accuracy of quantitative STEM measurements.

High-angle annular dark-field (HAADF) STEM imaging, based on elastic scattering of electrons, is quantitative since imaging intensity scales with atomic number ($I \propto Z^{1.7}$) [13]. Quantitative STEM imaging has been used to investigate dynamic metal electrodeposition [15], structural evolution of nanoscale electrocatalysts [9,16–19] and solid-electrolyte interphase formation of lithium batteries [20,21], among other energy applications [4,22]. HAADF-STEM imaging can maintain a high spatial resolution, particularly for high-Z nanoparticles in thick liquid, when compared to conventional bright-field (BF) TEM imaging [23,24]. The latest development in 4D-STEM significantly expands

the capability of STEM from conventional imaging to enable structural analysis in liquid [25,26]. 4D-STEM, based on electron microscopy pixel array detector (EMPAD), can achieve single electron sensitivity, high dynamic range and fast readout speed (up to 10,000 frames/second) [14], which are crucial for low-dose electron diffraction of beam-sensitive samples in liquid. While 4D-STEM diffraction imaging in vacuum has been demonstrated to achieve sub-Å real-space resolution and sub-pm reciprocal-space resolution [27], 4D-STEM in liquid has revealed valuable structural information already with nm-scale real-space resolution and sub-Å reciprocal-space resolution [9,16,17]. STEM based core-loss EELS signals (>50 eV) are compromised by multiple inelastic scattering in liquid and only resolvable when liquid layers are thinner than 200−300 nm below which mass transport for electrochemistry becomes challenging [23,24,28]. In comparison, valence EELS, below the optical gap of the electrolyte (about 1−6 eV), is effective to resolve features through liquid thickness up to 500−600 nm. *Operando* energy-filtered TEM imaging, based on valence EELS, was used to track rapid de-/lithiation dynamics of $LiFePO_4$ nanoparticles and corresponding concentration/depletion of the diffuse layer in liquid during battery cycles [24]. STEM-EDX analysis is particularly powerful for analyzing heavy elements due to the high penetration depth of X-rays through thick samples. Recent technical developments addressed the shadowing problem of the liquid-cell holder tip and enabled more X-rays to reach the EDX detector [29]. In addition, the equipment of dual or quadruple EDX detectors can achieve a high collection efficiency with a large solid angle of one Steradian or above, which can significantly lower the beam dose in order to achieve desirable nm-scale spatial resolution. When compared to the relatively slow scanning mode of STEM imaging, conventional bright field (BF) TEM imaging can serve as a complementary imaging mode to achieve a sub-second-level or higher temporal resolution with faster electron detectors. The spatial resolution of TEM imaging is limited by chromatic aberration due to multiple inelastic scattering in liquid [30], which can be mitigated through energy filtering or chromatic aberration correction [23]. Since the pioneering work by Ross et al. [31], TEM imaging has been widely used to probe interfacial electrochemical dynamics [32−36]. Selected area electron diffraction (SAED), despite the absence of spatial resolution, has been used to reveal valuable structural information on electroreduction of $Cu_2O$ nanoparticles [35]. TEM imaging and SAED have the merit of being widely accessible to most institutions as long as a conventional TEM is available. In general, electron diffraction is more dose efficient than S/TEM imaging for retrieving structural information of crystalline materials in liquid [13,14]. This review anticipates that the continuous development of STEM techniques in liquid, especially 4D-STEM diffraction imaging, will make significant contributions to the electrochemistry community.

*Operando* synchrotron X-ray methods have been developed over a long period of time and are instrumental in understanding electrochemical reactions at solid−liquid interfaces (Table 1). Hard XAS, including X-ray absorption near-edge structure (XANES) and extended X-ray absorption fine structure (EXAFS), is the most widely used *operando* X-ray method for reliably probing electrochemical reactions due to the high penetration depth and minimal beam damage [36−44]. Hard XAS excites core electrons of bulk samples, e.g. 3d metal K edges, and can be used to probe the site symmetry and oxidation state of an absorbing atom as well as the distances and identities of its nearest neighbors. For example, XAS can probe electrochemically induced surface changes of NPs, which are sufficient to trigger spectroscopic differences in XANES for quantitative analysis of valence states due to the high surface-to-bulk ratio of NPs. EXAFS, on the other hand, is more useful for detecting surface undercoordination for nanoparticles smaller than about 20 nm (one monolayer ($\sim$3 Å) of a 20 nm or larger spherical NP corresponds to less than 10% contribution from the surface) [9]. XANES of first−row transition metals, collected in transmission mode, has an edge energy resolution of $\sim$1.5 eV using a conventional solid-state detector with an energy resolution of 50−200 eV. The recent development of detecting XAS using a high resolution crystal spectrometer has given rise to high-energy-resolution fluorescence detected (HERFD) XAS, which enables much higher energy resolution—on the order of 0.5−0.75 eV— and allows for unprecedented information to be extracted from pre-edges [9,43−45]. This improved resolution comes at the price of signal intensity: While high quality HERFD XANES can be collected quickly, HERFD EXAFS requires significantly more time in order to achieve good SNR at high k for high resolution data. Hard X-ray diffraction, in particular crystal truncation rod (CTR) and X-ray standing waves (XSWs), enable an atomic-scale understanding of the electrode−electrolyte interfaces by decoupling surface changes from the bulk substrate. Both CTR and XSWs require well-defined, ideally single-crystal metal or oxide electrode surfaces [46,47]. Hard X-ray microscopy and correlative XRD have been used to penetrate mm-thick electrode samples and electrolytes and provided μm-level spatial resolution for dynamic de-/lithiation processes in batteries and oxygen evolution electrocatalysts [48−50]. In comparison to hard X-rays, soft XAS offers the twin advantages of producing much higher resolution spectra ($\sim$0.1 eV) and directly, via dipole-allowed transitions, probing the d orbital manifold of an absorbing 3d metal, which is sensitive to changes of metals' chemical environment. The main challenges facing soft X-ray studies are the beam-induced damage due to larger inelastic scattering cross

section and the design of vacuum-compatible liquid cells [51—55]. Soft XAS can be collected in either bulk-sensitive (hundreds of nm) total fluorescence yield (TFY) or surface-sensitive (<10 nm) total electron yield (TEY). Electron-yield XANES (EY-XANES) has been developed to probe interfacial water structure under electrochemical conditions [51]. Recently, *operando* resonant soft X-ray scattering (RSoXS) was developed to combine soft XAS studies of chemical environment and X-ray scattering of interparticle dynamics using a similar liquid-cell holder as EC-STEM [56]. Soft scanning transmission X-ray microscopy (STXM) was developed to provide nm-scale spatial resolution with simultaneous acquisition of an XAS spectrum [10,57]. Given an intense soft X-ray beam is focused into a nanoprobe, soft STXM has a high demand for sample stability in liquid under long-time beam exposure. Finally, *in situ* ambient pressure X-ray photoelectron spectroscopy (AP-XPS) can partially simulate electrochemical reaction conditions (a few torr with a thin liquid film) and has been reported to investigate chemical bonding on electrode surfaces [58].

*Operando* EC-STEM enables quantitative electrochemistry and simultaneous STEM imaging, 4D-STEM diffraction, EELS and EDX spectroscopy (Figure 1a) [9,15—17]. The central component of the EC-STEM is an electrochemical liquid cell with a three-electrode system of a carbon working electrode (WE), Pt counter and reference electrode (CE, RE, Figure 1b) [17]. A common EC-STEM holder often encapsulates electrolyte between two electron-transparent $SiN_x$ windows with a spacer of 500 nm. Figure 1c presents a cyclic voltammetric (CV) profile of Cu NPs with well-defined redox couple of $Cu_2O$/Cu with the conversion from Pt pseudo-RE to reversible hydrogen electrode (RHE) estimated to be around 0.8 V [17]. The natural formation of electrogenerated $H_2$ bubbles under reducing potentials generates a thin-liquid layer (~100 nm) that remains electrochemically accessible (Figure 1d) [16,17]. This unique strategy enables *operando* EC-STEM to expand beyond conventional imaging of morphological changes and allows for 4D-STEM, EELS and EDX analysis (Figure 1e—f) [14]. The first demonstration of *operando* 4D-STEM in liquid was performed to reveal crystallographic orientation mapping of Au—Pt bimetallic alloys during cathodic corrosion (Figure 1e). The thin-liquid layer also enables the acquisition of STEM-EDX mapping of heterogeneous Au—Pt nanostructures in liquid (Figure 1f). Recently, *operando* EC-STEM, equipped with 4D-STEM, and correlative X-ray methods were employed to elucidate a longstanding challenge of identifying Cu active sites for $CO_2$ reduction reaction ($CO_2$RR) to multicarbon products [9]. This study provides, for the first time, the definitive evidence of metallic Cu nanograins, rich in nanograin boundaries, supporting undercoordinated Cu active sites for C—C coupling (Figure 1g). *Operando* correlative methods provide a comprehensive life cycle of Cu nanocatalysts in which NP ensembles evolve into metallic Cu nanograins under $CO_2$RR before complete oxidation to single-crystal $Cu_2O$ nanocubes upon air exposure [9]. Two false-color *operando* 4D-STEM diffraction imaging in liquid shows the complex structure of metallic Cu nanograin boundaries as possible active sites for $CO_2$RR.

The customized electrochemical liquid-cell holder is compatible with not only *operando* EC-STEM but also resonant soft X-ray scattering (RSoXS, Figure 2a, c) [56]. *Operando* RSoXS provides a statistically robust analysis of dynamic aggregation processes of large ensembles of Cu NPs, complementing *operando* EC-STEM studies of individual Cu NPs. The major modification of the liquid-cell microchip for soft X-rays is the design of a dual carbon WE. Given the soft X-ray beam size is comparable to the electrode size, Cu NPs on window 1 are exposed to soft X-rays while those on window 2 experience the same electrochemical conditions but without X-ray exposure. Such a rigorous control experiment is essential to reliably investigate Cu@$Cu_2O$ NPs that are subject to rapid soft X-ray beam-induced oxidation to CuO in the electrolyte [56]. *Operando* RSoXS enables simultaneous acquisition of soft XAS to study valence state during electroreduction of $Cu_2O$ and X-ray scattering to study interparticle dynamics (Figure 2b, d). The NP-NP distance of 18 nm NP ensembles was measured to be 2.5 nm and decreased by 3 Å during $CO_2$RR. To accurately quantify valence state, HERFD was employed to enable hard X-rays with <1 eV-level energy resolution by exclusively selecting particular emission lines, such as Cu $K\alpha_1$, and thus suppressing the 1s core-hole lifetime broadening [4]. The pre-edge peaks are barely resolvable between Cu and $Cu_2O$ in conventional XANES (Figure 2e). In comparison, the pre-edge peaks in HERFD XANES become markedly different (8979.9 eV for Cu; 8981.0 eV for $Cu_2O$, Figure 2f). The pre-edge peak of CuO at 8977.6 eV is clearly shown in HERFD XANES but absent in conventional XANES. Quantitative analysis of *operando* HERFD XANES shows that all 7 nm NPs are converted to fully metallic Cu nanograins (Figure 2g—h) [9]. Such comprehensive multimodal *operando* methods represent a milestone in providing critical evidence of metallic Cu as active sites for $CO_2$RR. We anticipate that the continuous advances in *operando* X-ray methods, together with *operando* EC-STEM, will be instrumental in tackling the complex dynamic evolution of nanoscale electrocatalysts.

The level of impact of *operando* EC-STEM and X-ray methods on the electrochemistry community depends on how quantitatively we understand the electrochemical behaviors in liquid cells that are customized for *operando* measurements [17,21]. In order to encourage the general electrochemistry community to

**Figure 1**

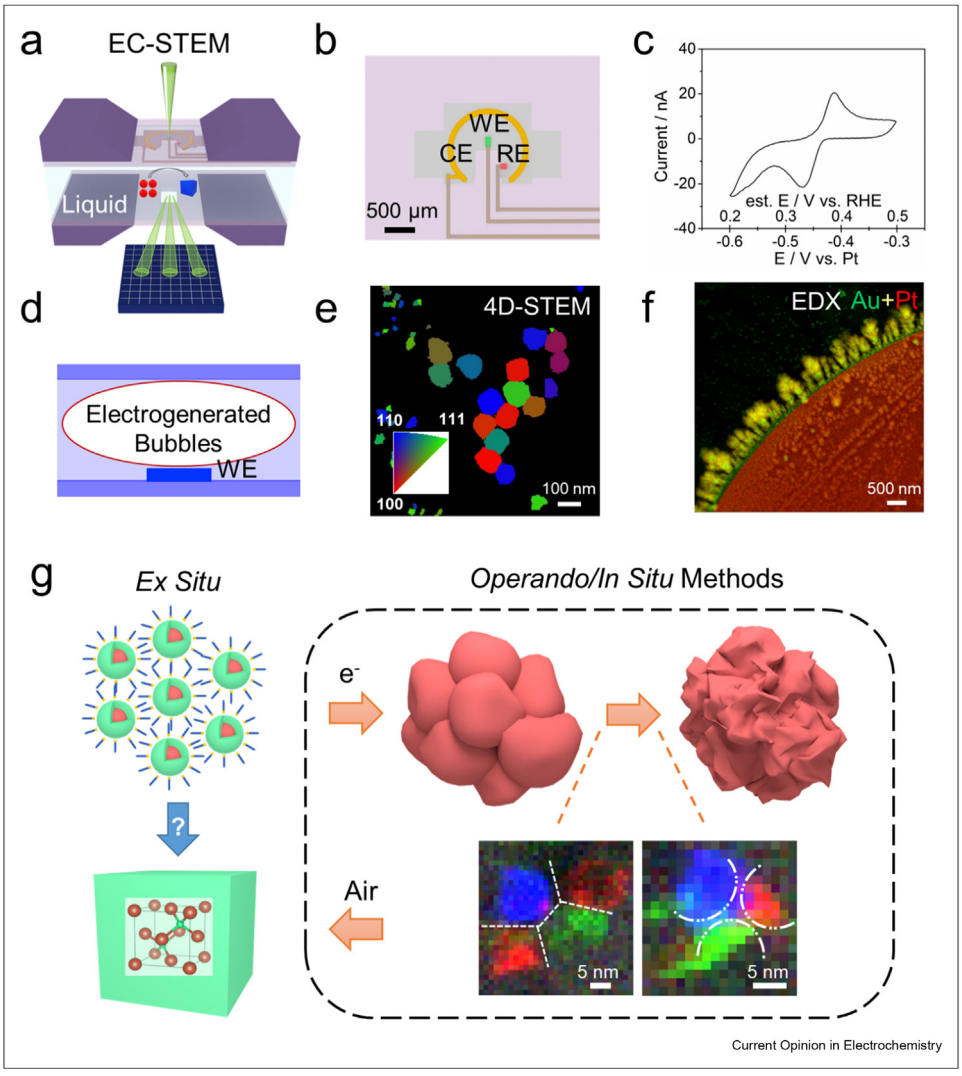


Selected examples of *operando* STEM under electrochemical conditions. (**a–c**) *Operando* EC-STEM setup with a three-electrode system and CV profiles of Cu NPs in $CO_2$-saturated 0.1 M $KHCO_3$ (adapted from a study by Yang et al. [17]. Copyright (2023) American Chemical Society). (**d–f**) Electrogenerated $H_2$ bubbles under reducing potentials create a native thin liquid layer (~100 nm), which enables 4D-STEM diffraction imaging (**e**) and STEM-EDX (**f**) of Au–Pt bimetallic alloys formed under electrochemical conditions (adapted from a study by Yang et al. [16]. Copyright (2022) American Chemical Society). (**g**) Compared to limited insights from *ex situ* methods, *operando/in situ* electrochemical 4D-STEM and correlative X-ray methods uncovered the dynamic evolution from Cu@$Cu_2O$ nanoparticles to metallic Cu nanograins under bias and transformation to $Cu_2O$ cubes upon air exposure (adapted from a study by Yang et al. [9]. Copyright (2023) Springer Nature).

adopt *operando* EC-STEM and X-ray methods, it is necessary to better understand how mass transport and kinetic equations of standard electrochemistry experiments change as a result of the unique geometry of *operando* cells, *i.e.* it is necessary to benchmark electrochemistry in confined and heterogenous liquid layers. Figure 3a presents the well-defined redox couple of Cu electrodeposition and stripping on Au nanocube electrode surfaces as a function of scan rate. A log–scale plot of the reduction peak current vs. scan rate shows a square-root relation, which is characteristic of a diffusion-controlled process [15]. Further analysis based on the Randles–Ševčík equation estimated the diffusion coefficient of $Cu^{2+}$ to be $3.4 \times 10^{-5}$ $cm^2/s$. This is within the same order of magnitude when compared to the value reported in the literature ($7.4\times 10^{-6}$ $cm^2/s$) for 1 mM $Cu^{2+}$ in standard (bulk) cells, which suggests that the microelectrode in EC-STEM shows a bulk diffusion behavior, despite the confined sub-μm thick liquid layer [15]. The window bulging, a result of pressure differences between the liquid cell and the TEM chamber, makes the liquid thicker in the middle of the window and, thus, more challenging to resolve nanoscale features (Figure 3b) [20]. Liquid thickness

**Figure 2**

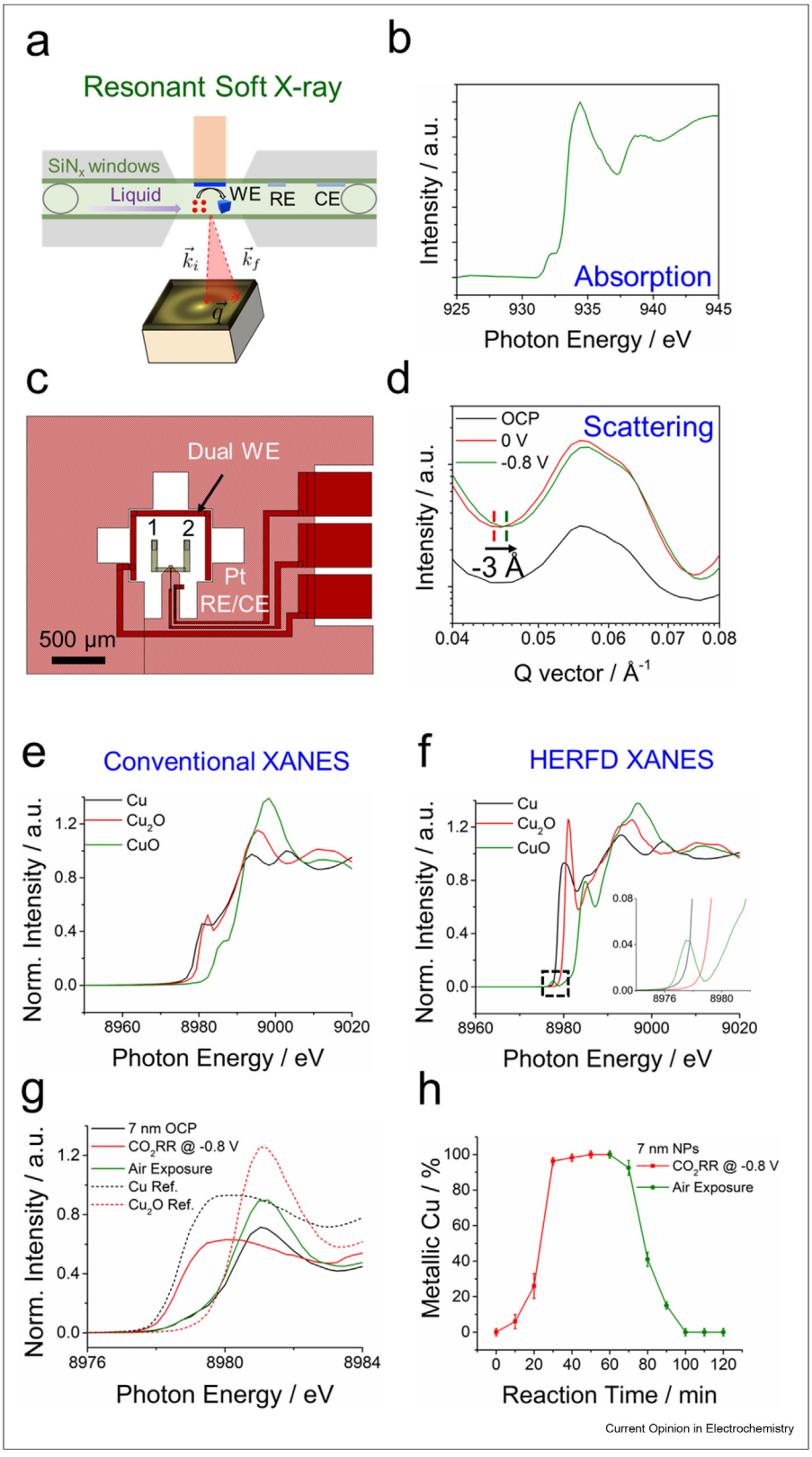


Selected examples of *operando* soft and hard X-ray methods under electrochemical conditions. (**a–b**) *Operando* RSoXS using the same liquid-cell holder as EC-STEM with a three-electrode system including a dual carbon WE. (**c–d**) *Operando* RSoXS enables the simultaneous acquisition of soft XAS and X-ray scattering (Figures a–d were adapted from a study by Yang et al. [56]. Copyright (2022) American Chemical Society). (**e**) Working principle of HERFD XAS (f–g) Comparison of XANES spectra of Cu, $Cu_2O$ and CuO in conventional and HERFD modes. Inset in (**f**) showing the presence of a unique pre-peak of CuO only detectable in HERFD mode (Figures e–h were adapted from a study by Yang et al. [9]. Copyright (2023) Springer Nature).

**Figure 3**

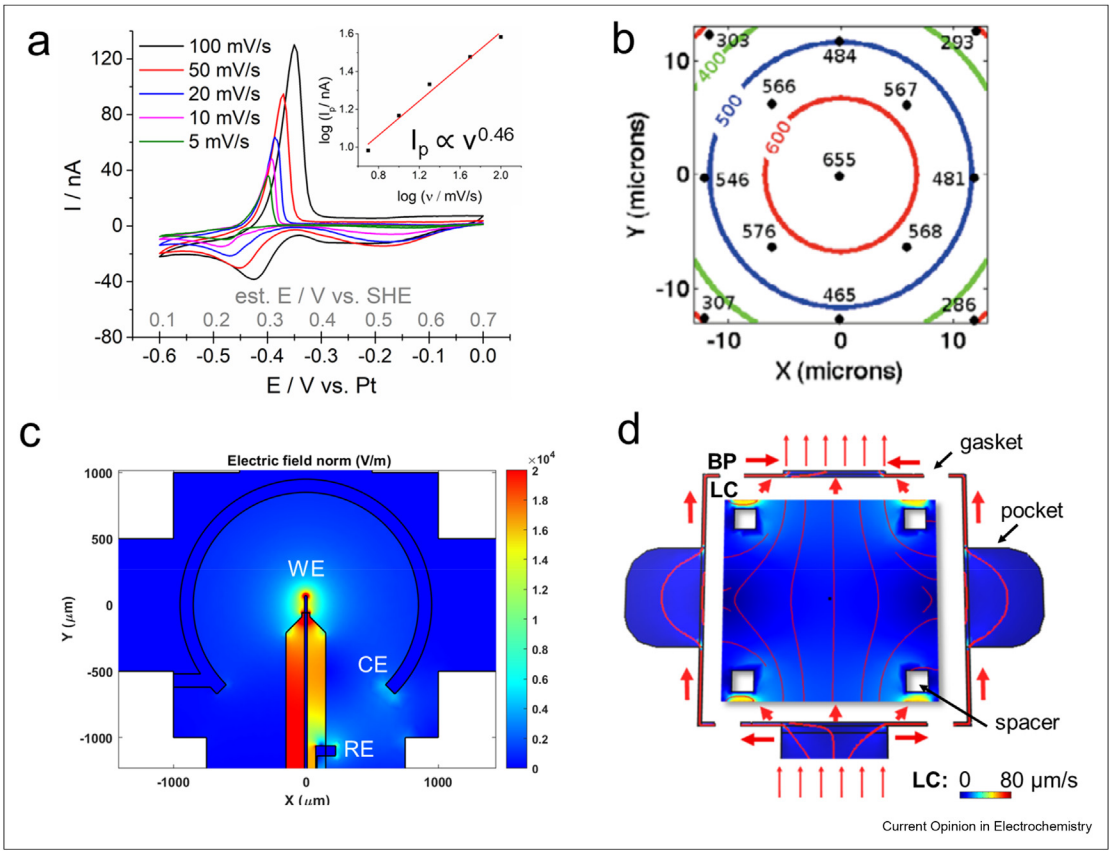


Benchmark electrochemistry in confined and heterogenous liquid environment. (**a**) CV profiles of Cu electrodeposition and stripping in 1 mM $CuSO_4$/0.1 M $NaClO_4$ in EC-STEM holder (adapted from a study by Yang et al. [15]. Copyright (2022) American Chemical Society). (**b**) EELS measurements of liquid thickness variation for water with a 150 nm spacer in between two 25 × 25 $\mu m^2$ $SiN_x$ windows (adapted from a study by Holtz et al. [20]. Copyright (2013) Microscopy Society of America). (**c**) Finite element simulation of the heterogeneous electric field distribution in vacuum of a three-electrode system with a WE potential of −1 V vs. RHE and CE potential of 2 V vs. RHE (Copyright by the authors). (**d**) Numerically simulated flow velocity profile of a liquid cell (LC) with realistic consideration of 2% off-chip bypass (BP) and a spacer of 150 nm. Red lines indicate direction and background color represents relative magnitude of flow velocity. The black square in the center reflects 20 × 20 $\mu m^2$ viewing window (adapted from a study by Merkens et al. [62]. Copyright (2023) Elsevier). (For interpretation of the references to color in this figure legend, the reader is referred to the Web version of this article.)

can be estimated using the plasmon peak in the EELS spectrum and applying Beer's Law. The strategy of electrogenerated $H_2$ bubbles works well for electrochemical applications under reducing potentials [16,17], but there is a need to advance nanofabrication for a pristine liquid layer of 100 nm or thinner without forming gas bubbles [59].

In confined liquid cells, the electric field distribution and liquid flow are spatially heterogeneous [4,21]. Figure 3c shows the electric field map of the three-electrode system in vacuum using finite element simulations assuming a typical $CO_2$RR condition with a WE potential of −1 V vs. RHE (reversible hydrogen electrode). The significantly higher electric field around the tip of the WE has a profound tip-enhanced effect on the evolution dynamics of nanoparticles. Recent liquid-cell TEM studies show pronounced aggregation of nanoscale features at the edge or tip of the WE while particle evolution in the central part of the WE shows a more homogenous and better potential-dependent control [9,34]. Thus, we emphasize the need to report the relative imaging location in the electrochemical chip and make close comparisons between evolution dynamics in liquid-cell STEM and that in standard electrochemical cells. Liquid flow is typically applied for continuous supply of fresh electrolyte and/or removal of species created in electrochemical (or radiolytic) processes in the liquid cell, but also allows to change the composition through solution replacement and *in situ* mixing [30,59–61]. Solute diffusion is an inherent mass transport mechanism induced by concentration gradients arising either due to external supply of solutes or their local generation during (electro-)chemical reactions. Figure 3d presents the hydrodynamic quantification of a realistic liquid-cell flow setup based on its

experimentally validated 3D flow channel geometry and reveals significant heterogeneity in mass transport rates across the nanochannel [62]. The relative velocity is noticeably higher on the side of the microchip than the middle region with realistic consideration of liquid bypassing along the chip edge. Continuous development of new liquid-cell geometries will provide EC-STEM setups with a well-defined mass transport and microfluidic dynamics [63].

In conclusion, this review summarizes recent advances in developing *operando* STEM based imaging, 4D-STEM diffraction, EELS and EDX spectroscopy, and correlative synchrotron hard and soft X-ray based absorption, diffraction, scattering and microscopy in liquid under electrochemical conditions. Multimodal *operando* EC-STEM and X-ray methods have been demonstrated to serve as complementary probes to elucidate the complex nature of active sites and dynamic evolution at unprecedented spatiotemporal resolutions. We emphasize the importance of demonstrating faithful electrochemical results in liquid cells without interference of beam-induced damage and the need for close comparisons to standard electrochemical measurements. We lay out several key points for *operando* EC-STEM and correlative X-ray methods to be widely accessible with simple and reliable operation for the broad chemistry and energy materials community:

(1) The spatial resolution of STEM in liquid is often limited to a few nanometers by maximum beam dose applied to samples rather than instrument resolutions. The low beam dose (a few $e^{-}/Å^{2}$) in EC-STEM often requires a beam current of a few pA or lower [9,15–17,24]. Thus, EC-STEM has the potential to be widely applicable with a more affordable non-aberration-corrected STEM and a normally bright electron gun instead of an expensive aberration-corrected STEM with a very bright electron gun. Additional benefits of non-aberration-corrected STEM are a larger depth of focus [64], particularly useful for thick liquid samples, and easier alignment and maintenance for general use.
(2) Quantification of electrochemistry by developing standard reference electrodes with mV-level potential stability to replace Pt pseudo RE [65].
(3) Correlations of multimodal *operando* methods across fields: Correlation of individual STEM and/or X-ray techniques, correlation of electrons and X-rays as structural probes with molecular probes (vibrational spectroscopy) [1,5,8], online product detection (DEMS) [9,66,67], online inductively coupled plasma (ICP) MS [68] and local activity (SECM) [10,69,70]. This combined approach will contribute to elucidating complex structural evolution under realistic electrochemical conditions, which otherwise will be impossible to comprehend with individual techniques [11,71].
(4) Synchronization of electrochemical measurements with EC-STEM or X-ray data acquisition with the development of integrated and automated data processing software.
(5) Rapid processing and feedback of large 4D-STEM and X-ray datasets as the demand for spatial and temporal resolutions continues to increase the data size, which has the potential to incorporate the latest developments in machine learning [72].

## Declaration of competing interest

The authors declare that they have no known competing financial interests or personal relationships that could have appeared to influence the work reported in this paper.

## Data availability

Data will be made available on request.

## Acknowledgments

This work was supported by Director, Office of Science, Office of Basic Energy Sciences, Chemical Sciences, Geosciences, & Biosciences Division, of the U.S. Department of Energy under Contract DE-AC02- 05CH11231, FWP CH030201 (Catalysis Research Program). Work at Cornell University (especially *operando* EC-STEM) was supported by the Center for Alkaline-Based Energy Solutions (CABES), an Energy Frontier Research Center (EFRC) program supported by the U.S. Department of Energy, under grant DE–SC0019445. This work made use of TEM facilities at the CCMR which are supported through the National Science Foundation Materials Research Science and Engineering Center (NSF MRSEC) program (DMR-1719875). This work also used TEM facilities at the Molecular Foundry was supported by the Office of Science, Office of Basic Energy Sciences, of the U.S. Department of Energy under Contract No. DE-AC02-05CH11231. This research used resources of the Advanced Light Source, which is a DOE office of Science User Facility under contract no. DE-AC02- 05CH11231. This work is based on research conducted at the Center for High-Energy X-ray Sciences (CHEXS), which is supported by the National Science Foundation (BIO, ENG and MPS Directorates) under award DMR-1829070.

## References

Papers of particular interest, published within the period of review, have been highlighted as:

* of special interest
** of outstanding interest

1. Yang Y, *et al.*: **Electrocatalysis in alkaline media and alkaline membrane-based energy technologies**. *Chem Rev* 2022, **122**: 6117–6321, https://doi.org/10.1021/acs.chemrev.1c00331.

2. Ross MB, Luna PD, Li Y, Dinh C-T, Kim D, Yang P, Sargent EH: **Designing materials for electrochemical carbon dioxide recycling**. *Nat Catal* 2019, **2**:648–658, https://doi.org/10.1038/s41929-019-0306-7.

3. Abruña HD: *Electrochemical interface: modern techniques for* in situ *interface characterization*. New York: VCH; 1991.

4. Yang Y, Xiong Y, Zeng R, Lu X, Krumov M, Huang X, Xu W, Wang H, DiSalvo FJ, Brock JD, Muller DA, Abruña HD: ***Operando* methods in electrocatalysis**. *ACS Catal* 2021, **11**:1136–1178, https://doi.org/10.1021/acscatal.0c04789.

5. Bentley CL, Kang M, Unwin PR: **Nanoscale surface structure–activity in electrochemistry and electrocatalysis**. *J Am Chem Soc* 2019, **141**:2179–2193. https://pubs.acs.org/doi/10.1021/jacs.8b09828.

6. Stevenson KJ, Tschulik KA: **Materials driven approach for understanding single entity nano impact electrochemistry**. *Curr*

*Opin Electrochem* 2017, **6**:38–45, https://doi.org/10.1016/j.coelec.2017.07.009.

7. Bañares MA: ***Operando* methodology: combination of *in situ* spectroscopy and simultaneous activity measurements under catalytic reaction conditions**. *Catal Today* 2005, **100**: 71–77, https://doi.org/10.1016/j.cattod.2004.12.017.

8. Weckhuysen BM: **Snapshots of a working catalyst: possibilities and limitations of *in situ* spectroscopy in the field of heterogeneous catalysis**. *Chem Commun* 2002:97–110, https://doi.org/10.1039/B107686H.

9. ** Yang Y, Louisia S, Yu S, Jin J, Roh I, Chen C, Fonseca Guzman MV, Feijóo J, Chen P, Wang H, Pollock CJ, Huang X, Shao Y-T, Wang C, Muller DA, Abruña HD, Yang P: ***Operando* studies reveal active Cu nanograins for $CO_2$ electroreduction**. *Nature* 2023, **614**:262–269, https://doi.org/10.1038/s41586-022-05540-0.
This work employs *operando* EC-STEM, 4D-STEM and correlative hard and soft X-ray methods and provides, for the first time, definitive evidence on metallic Cu nanograins as active sites for $CO_2$.

10. Mefford JT, Akbashev AR, Kang M, Bentley CL, Gent WE, Deng HD, Alsem DH, Yu Y-S, Salmon NJ, Shapiro DA, Unwin PR, Cheuh WC: **Correlative *operando* microscopy of oxygen evolution electrocatalysts**. *Nature* 2021, **593**:67–73, https://doi.org/10.1038/s41586-021-03454-x.

11. van der Stam W: **The necessity for multiscale *in situ* characterization of tailored electrocatalyst nanoparticle stability**. *Chem Mater* 2023, **35**:386–394, https://doi.org/10.1021/acs.chemmater.2c03286.

12. de Jonge N, Houben L, Dunin-Borkowski RE, Ross FM: **Resolution and aberration correction in liquid cell transmission electron microscopy**. *Nat Rev Mater* 2019, **4**:61–78, https://doi.org/10.1038/s41578-018-0071-2.

13. Muller DA: **Structure and bonding at the atomic scale by scanning transmission electron microscopy**. *Nat Mater* 2009, **8**:263–270, https://doi.org/10.1038/nmat2380.

14. Philipp HT, Tate MW, Shanks KS, Mele L, Peemen M, Dona P, Hartong R, van Veen R, Shao YT, Chen Z, Thom-Levy J, Muller DA, Gruner SM: **Very-high dynamic range, 10,000 frames/second pixel array detector for electron microscopy**. *Micro. Microanal* 2022, **28**:425–440, https://doi.org/10.1017/S1431927622000174.

15. Yang Y, Shao Y-T, Lu X, DiSalvo FJ, Abruña HD, Muller DA: **Metal monolayers on command: underpotential deposition at nanocrystal surfaces: a quantitative *operando* electrochemical transmission electron microscopy study**. *ACS Energy Lett* 2022, **7**:1292–1297, https://doi.org/10.1021/acsenergylett.2c00209.

16. ** Yang Y, Shao Y-T, Lu X, Yang Y, Ko HY, DiStasio RA, DiSalvo FJ, Muller DA, Abruña HD: **Elucidating cathodic corrosion mechanisms with *operando* electrochemical transmission electron microscopy**. *J Am Chem Soc* 2022, **144**: 15698–15708, https://doi.org/10.1021/jacs.2c05989.
This work demonstrates the first 4D-STEM in liquid.

17. Yang Y, Shao Y-T, Jin J, Feijóo J, Roh I, Louisia S, Yu S, Fonseca Guzman MV, Chen C, Muller DA, Abruña HD, Yang P: ***Operando* electrochemical liquid-cell scanning transmission electron microscopy (EC-STEM) studies of evolving Cu nanocatalysts for $CO_2$ electroreduction**. *ACS Sustainable Chem Eng* 2023, **11**: 4119–4124, https://doi.org/10.1021/acssuschemeng.2c06542.

18. Yoon A, Grosse P, Rettenmaier C, Herzog A, Chee SW, Roldan Cuenya B: **Dynamic transformation of cubic copper catalysts during $CO_2$ electroreduction and its impact on catalytic selectivity**. *Nat Commun* 2021, **12**:6736, https://doi.org/10.1038/s41467-021-27500-4.

19. Beermann V, Holtz ME, Padgett E, de Araujo JF, Muller DA, Strasser P: **Real-time imaging of activation and degradation of carbon supported octahedral Pt–Ni alloy fuel cell catalysts at the nanoscale using in situ electrochemical liquid cell STEM**. *Energy Envion Sci* 2019, **12**:2476–2485, https://doi.org/10.1039/C9EE01185D.

20. Sacci RL, Black JM, Balke N, Dudney NJ, More KL, Unocic RR: **Nanoscale imaging of fundamental Li battery chemistry: solid-electrolyte interphase formation and preferential growth of lithium metal nanoclusters**. *Nano Lett* 2015, **15**: 2011–2018, https://doi.org/10.1021/nl5048626.

21. Bhatia A, *et al.*: **In Situ liquid electrochemical TEM investigation of $LiMn_{1.5}Ni_{0.5}O_4$ thin film cathode for micro-battery applications**. *Small Methods* 2022, **6**:2100891, https://doi.org/10.1002/smtd.202100891.

22. * Unocic RR, Sacci RL, Brown GM, Veith GM, Dudney NJ, More KM, Walden II FS, Gardiner DS, Damiano J, Nackashi DP: **Quantitative electrochemical measurements using in situ EC-S/TEM devices**. *Microsc Microanal* 2014, **20**:452–461, https://doi.org/10.1017/S1431927614000166.
This work is one of the earliest reports on a systematic study of effects of electrode geometry and microfluidic conditions on electrochemical measurements.

23. ** Holtz ME, Yu Y, Gao J, Abruña HD, Muller DA: ***In situ* electron energy-loss spectroscopy in liquids**. *Microsc Microanal* 2013, **19**:1027–1035, https://doi.org/10.1017/S1431927613001505.
This work remains a must-read on core-loss and valence-loss EELS in liquid.

24. Holtz ME, Yu Y, Gunceler D, Gao J, Sundararaman R, Schwarz KA, Arias TA, Abruña HD, Muller DA: **Nanoscale imaging of lithium ion distribution during *in situ* operation of battery electrode and electrolyte**. *Nano Lett* 2014, **14**: 1453–1459, https://doi.org/10.1021/nl404577c.

25. Tate MW, Purohit P, Chamberlain D, Nguyen KX, Hovden R, Chang CS, Deb P, Turgut E, Heron JT, Schlom DG, Ralph D, Fuchs GD, Shanks KS, Philipp HT, Muller DA, Gruner SM: **High dynamic range pixel array detector for scanning transmission electron microscopy**. *Microsc Microanal* 2016, **22**: 237–249, https://doi.org/10.1017/S1431927615015664.

26. Chen Z, Jiang Y, Shao YT, Holtz ME, Odstrcil M, Guizar-Sicairos M, Hanke I, Ganschow S, Schlom DG, Muller DA: **Electron ptychorgraphy achieves atomic-resolution limits set by lattice vibrations**. *Science* 2021, **372**:826–831, https://doi.org/10.1126/science.abg2533.

27. Padgett E, Holtz ME, Cueva P, Shao YT, Langenberg E, Schlom DG, Muller DA: **The exit-wave power-cepstrum transform for scanning nanobeam electron diffraction: robust strain mapping at subnanometer resolution and subpicometer precision**. *Ultramicroscopy* 2020, **214**:112994, https://doi.org/10.1016/j.ultramic.2020.112994.

28. Serra-Maia R, Kumar P, Meng AC, Foucher AC, Kang Y, Karki K, Jariwala D, Stach EA: **Nanoscale chemical and structural analysis during in situ scanning/transmission electron microscopy in liquids**. *ACS Nano* 2021, **15**:10228–10240, https://doi.org/10.1021/acsnano.1c02340.

29. Lewis E, Haigh SJ, Slater TJA, He Z, Kulzick MA, Burke MG, Zaluzec NJ: **Real-time imaging and local elemental analysis of nanostructures in liquids**. *Chem Commun* 2014, **50**: 10019–10022, https://doi.org/10.1039/C4CC02743D.

30. Klein KL, Anderson IM, de Jonge N: **Transmission electron microscopy with a liquid flow cell**. *J Microsc* 2011, **242**: 117–123, https://doi.org/10.1063/1.4754271.

31. * Williamson M, Tromp R, Vereecken P, Hull R, Ross FM: **Dynamic microscopy of nanoscale cluster growth at the solid–liquid interface**. *Nat Mater* 2003, **2**:532–536, https://doi.org/10.1038/nmat944.
This study is the pioneering work demonstrating the feasibility of an electrochemical liquid-cell TEM using a two-electrode configuration.

32. Zeng Z, Zhang X, Bustillo K, Niu K, Gammer C, Xu J, Zheng H: **In situ study of lithiation and delithiation of $MoS_2$ nanosheets using electrochemical liquid cell transmission electron microscopy**. *Nano Lett* 2015, **15**:5214–5220, https://doi.org/10.1021/acs.nanolett.5b02483.

33. Li Y, Kim D, Louisia S, Xie C, Kong Q, Yu S, Lin T, Aloni S, Fakra S, Yang P: **Electrochemically scrambled nanocrystals are catalytically active for $CO_2$-tomulticarbons**. *Proc Natl Acad Sci USA* 2020, **117**:9194–9201, https://doi.org/10.1073/pnas.1918602117.

34. Wang X, Klingan K, Klingenhof M, Möller T, de Araújo JF, Martens I, Bagger A, Jiang S, Rossmeisl J, Dau H, Strasser P:

**Morphology and mechanism of highly selective Cu(II) oxide nanosheet catalysts for carbon dioxide electroreduction**. *Nat Commun* 2021, **12**:794, https://doi.org/10.1038/s41467-021-20961-7.

35. Vavra J, Shen TH, Stoian D, Tileli V, Buonsanti R: **Real-time monitoring reveals dissolution/redeposition mechanism in copper nanocatalysts during the initial stages of the $CO_2$ reduction reaction**. *Angew Chem Int Ed* 2021, **60**:1347–1354, https://doi.org/10.1002/anie.202011137.

36. Peña, *et al.*: **Morphological and structural evolution of $Co_3O_4$ nanoparticles revealed by in situ electrochemical transmission electron microscopy during electrocatalytic water oxidation**. *ACS Nano* 2019, **13**:11372, https://doi.org/10.1021/acsnano.9b04745.

37. * Yang Y, Wang Y, Xiong Y, Huang X, Shen L, Huang R, Wang H, Pastore JP, Yu S-H, Xiao L, Brock JD, Zhuang L, Abruña HD: ***In situ* X-ray absorption spectroscopy of a synergistic Co-Mn oxide catalyst for the oxygen reduction reaction**. *J Am Chem Soc* 2019, **141**:1463–1466, https://doi.org/10.1021/jacs.8b12243.
This study is the first *operando* XAS study of the synergistic effect of co-active sites in bimetallic oxides with a 3 mV potential resolution for tracking reaction dynamics.

38. Xiong Y, Yang Y, Feng X, DiSalvo FJ, Abruña HD: **A strategy for increasing the efficiency of the oxygen reduction reaction in Mn-doped cobalt ferrites**. *J Am Chem Soc* 2019, **141**:4412–4421, https://doi.org/10.1021/jacs.8b13296.

39. Zeng R, Yang Y, Feng X, Li H, Gibbs LM, DiSalvo FJ, Abruña HD: **Nonprecious transition metal nitrides as efficient oxygen reduction electrocatalysts for alkaline fuel cells**. *Sci Adv* 2022, **8**:eabj1584, https://doi.org/10.1126/sciadv.abj1584.

40. Chang C-J, Lin S-C, Chen H-C, Wang J, Zheng KJ, Zhu Y, Chen HM: **Dynamic reoxidation/reduction-driven atomic interdiffusion for highly selective $CO_2$ reduction toward methane**. *J Am Chem Soc* 2020, **142**:12119–12132, https://doi.org/10.1021/jacs.0c01859.

41. Li J, *et al.*: **Copper adparticle enabled selective electrosynthesis of n-propanol**. *Nat Commun* 2018, **9**:4614, https://doi.org/10.1038/s41467-018-07032-0.

42. Kimura KW, Casebolt R, DaSilva JC, Kauffman E, Kim J, Dunbar TA, Pollock CJ, Suntivich J, Hanrath T: **Selective electrochemical $CO_2$ reduction during pulsed potential stems from dynamic interface**. *ACS Catal* 2020, **10**:8632–8639, https://doi.org/10.1021/acscatal.0c02630.

43. Friebel D, *et al.*: **Identification of highly active Fe sites in (Ni,Fe)OOH for electrocatalytic water splitting**. *J Am Chem Soc* 2015, **137**:1305–1313, https://doi.org/10.1021/ja511559d.

44. Hung S-F, Chan Y-T, Chang C-C, Tsai M-K, Liao Y-F, Hiraoka N, Hsu C-S, Chen HM: **Identification of stabilizing high-valent active sites by *operando* high-energy resolution fluorescence-detected X-ray absorption spectroscopy for high-efficiency water oxidation**. *J Am Chem Soc* 2018, **140**:17263–17270, https://doi.org/10.1021/jacs.8b10722.

45. Hämäläinen K, Siddons DP, Hastings JB, Berman LE: **Elimination of the inner-shell lifetime broadening in X-ray-absorption spectroscopy**. *Phys Rev Lett* 1991, **67**:2850–2853, https://doi.org/10.1103/PhysRevLett.67.2850.

46. Plaza M, Huang X, Ko JYP, Shen M, Simpson BH, Rodríguez-López J, Ritzert NL, Letchworth-Weaver K, Gunceler D, Schlom DG, Arias TA, Brock JD, Abruña HD: **Structure of the photo-catalytically active surface of $SrTiO_3$**. *J Am Chem Soc* 2016, **138**:7816–7819, https://doi.org/10.1021/jacs.6b03338.

47. Abruña HD, Bommarito GM, Acevedo D: **The study of solid/liquid interfaces with X-ray standing waves**. *Science* 1990, **250**:69–74, https://doi.org/10.1126/science.250.4977.69.

48. Yu S-H, Huang X, Brock JD, Abruña HD: **Regulating key variables and visualizing lithium dendrite growth: an *operando* X-ray study**. *J Am Chem Soc* 2019, **141**:8441–8449, https://doi.org/10.1021/jacs.8b13297.

49. Yu S-H, Huang X, Schwarz K, Huang R, Arias TA, Brock JD, Abruña HD: **Direct visualization of sulfur cathodes: new insights into Li-S batteries via *operando* X-ray based methods**. *Energy Environ Sci* 2018, **11**:202–210, https://doi.org/10.1039/c7ee02874a.

50. Kuai C, Xi C, Hu A, Zhang Y, Xu Z, Nordlund D, Sun C-J, Cadigan CA, Richards RM, Li L, Dong C-K, Du X-W, Lin F: **Revealing the dynamics and roles of iron incorporation in nickel hydroxide water oxidation catalysts**. *J Am Chem Soc* 2021, **143**:18519–18526, https://doi.org/10.1021/jacs.1c07975.

51. Velasco-Velez J-J, Wu CH, Pascal TA, Wan LF, Guo J, Prendergast D, Salmeron MB: **The structure of interfacial water on gold electrodes studied by X-Ray absorption spectroscopy**. *Science* 2014, **346**:831–834. https://www.science.org/doi/10.1126/science.1259425.

52. Ye Y, Wu CH, Zhang L, Liu Y-S, Glans-Suzuki P, Guo J: **Using soft X-ray absorption spectroscopy to characterize electrode/electrolyte interfaces *in-situ* and *operando***. *J Electron Spectrosc Relat Phenom* 2017, **221**:2–9, https://doi.org/10.1016/j.elspec.2017.05.002.

53. Drake IJ, Liu TCN, Gilles M, Tyliszczak T, Kilcoyne ALD, Shuh DK, Mathies RA, Bell AT: **An *in situ* cell for characterization of solids by soft X-ray absorption**. *Rev Sci Instrum* 2004, **75**:3242, https://doi.org/10.1063/1.1791320.

54. Schwanke C, Xi L, Lange KM: **A Soft XAS transmission cell for operando studies**. *J Synchrotron Radiat* 2016, **23**:1390, https://doi.org/10.1107/S1600577516014697.

55. Weatherup RS, Wu CH, Escudero C, Pérez-Dieste V, Salmeron MB: **Environment-dependent radiation damage in atmospheric pressure x-ray spectroscopy**. *J Phys Chem B* 2018, **122**:737–744, https://doi.org/10.1021/acs.jpcb.7b06397.

56. * Yang Y, Roh I, Louisia S, Yu S, Chen C, Jin J, Yu S, Salmeron MB, Wang C, Yang P: ***Operando* resonant soft X-ray scattering studies of chemical environment and interparticle dynamics of cu nanocatalysts for $CO_2$ electroreduction**. *J Am Chem Soc* 2022, **144**:8927–8931, https://doi.org/10.1021/jacs.2c03662.
This work is the first demonstration of electrochemical RSoXS and systematically investigates the soft X-ray beam-induced oxidation of Cu in liquid environments.

57. Zhang C, Mille N, Eraky H, Stanescu S, Swaraj S, Belkhou R, Higgins D, Hitchcock A: **Copper $CO_2$ reduction electrocatalysts studied by in situ soft X-ray spectro-ptychography**. *ChemRXiv* 2023, https://doi.org/10.26434/chemrxiv-2023-67dt2.

58. Favaro M, Jeong B, Ross PN, Yano J, Hussain Z, Liu Z, Crumlin EJ: **Unravelling the electrochemical double layer by direct probing of the solid/liquid interface**. *Nat Commun* 2016, **7**:12695, https://doi.org/10.1038/ncomms12695.

59. Beker AF, Sun H, Lemang M, van Omme JT, Spruit RG, Bremmer M, Basak S, Pérez-Garza HH: **In situ electrochemistry inside a TEM with controlled mass transport**. *Nanoscale* 2020, **12**:22192–22201, https://doi.org/10.1039/D0NR04961A.

60. Schneider NM, Norton MM, Mendel BJ, Grogan JM, Ross FM, Bau HH: **Electron-water interactions and implications for liquid cell electron microscopy**. *J Phys Chem C* 2014, **118**:22373–22382.

61. Merkens S, De Salvo G, Chuvilin A: **The effect of flow on radiolysis in liquid phase-TEM flow cells**. *Nano Express* 2022, **3**:45006, https://doi.org/10.1088/2632-959X/acad18.

62. * Merkens S, De Salvo G, Kruse J, Modin E, Tollan C, Grzelczak M, Chuvilin A: **Quantification of reagent mixing in liquid flow cells for liquid phase-TEM**. *Ultramicroscopy* 2023, **245**:113654, https://doi.org/10.1016/j.ultramic.2022.113654.
This study establishes realistic hydrodynamic models of microfluidic channels in confined liquid cells.

63. Merkens S, Tollan C, De Salvo G, Bejtka K, Fontana M, Chiodoni A, Grzelczak M, Seifert A, Chuvilin A: **Towards sub-second solution exchange dynamics in liquid-phase TEM flow reactors**. *Research Square Preprint* 2023, https://doi.org/10.21203/rs.3.rs-3208774/v1.

64. Xin HL, Muller DA: **Aberration-corrected ADF-STEM depth sectioning and prospects for reliable 3D imaging in S/TEM**.

*J Electron Microsc* 2009, **58**:157–165, https://doi.org/10.1093/jmicro/dfn029.

65. Walker NL, Dick JE: **Leakless bipolar reference electrode: fabrication performance and miniaturization**. *Anal Chem* 2021, **93**:10065–10074, https://doi.org/10.1021/acs.analchem.1c00675.

66. Baltruschat H: **Differential electrochemical mass spectrometry**. *J Am Soc Mass Spectrom* 2004, **15**:1693–1706, https://doi.org/10.1016/j.jasms.2004.09.011.

67. Wang H, Abruña HD: **New insights into methanol and formic acid electro-oxidation on Pt: simultaneous DEMS and ATR-SEIRAS study under well-defined flow conditions and simulations of CO spectra**. *J Chem Phys* 2022, **156**, 034703, https://doi.org/10.1063/5.0071463.

68. Fuchs T, Briega-Martos V, Drnec J, Stubb N, Martens I, Calle-Vallejo F, Harrington DA, Cherevko S, Magnussen OM: **Anodic and cathodic platinum dissolution processes involve different oxide species**. *Angew Chem Int Ed* 2023, **62**, e202304293, https://doi.org/10.1002/anie.202304293.

69. Mariano RG, McKelvey K, White HS, Kanan MW: **Selective increase in $CO_2$ electroreduction activity at grain-boundary surface terminations**. *Science* 2017, **358**:1187–1192, https://doi.org/10.1126/science.aao3691.

70. Santos CS, Jaato BN, Sanjana I, Schuhmann W, Andronescu C: **Operando scanning electrochemical probe microscopy during electrocatalysis**. *Chem Rev* 2023, **123**:4972–5019, https://doi.org/10.1021/acs.chemrev.2c00766.

71. Abdi, *et al.*: **Understanding the dynamics of molecular water oxidation catalysts with liquid-phase transmission electron microscopy: the case of Vitamin $B_{12}$**. *ACS Sustainable Chem Eng* 2021, **9**:9494–9505, https://doi.org/10.1021/acssuschemeng.1c03539.

72. Shi C, Cao MC, Rehn SM, Bae S-H, Kim J, Jones MR, Muller DA, Han Y: **Uncovering material deformations via machine learning combined with four-dimensional scanning transmission electron microscopy**. *npj Comput Mater* 2022, **8**:114, https://doi.org/10.1038/s41524-022-00793-9.